https://doi.org/10.1016/j.ijrmhm.2017.10.006

A systematic investigation on the diamond wear mechanism during the dry scratching of WC/Co

Quanli Zhang[1*], Qingliang Zhao[2*], Honghua Su[1] and Suet To[3]

[1] *College of Mechanical and Electrical Engineering, Nanjing University of Aeronautics and Astronautics, Nanjing, 210016, China*

[2] *Centre for Precision Engineering, School of Mechatronics Engineering, Harbin Institute of Technology, Harbin, 150001, China*

[3] *State Key Laboratory of Ultra-precision Machining Technology, The Hong Kong Polytechnic University, Hong Kong*

*Corresponding Author / E-mail: zhangql606@163.com, TEL: +86-025-84895857, FAX: +86-025-84895857

zhaoqingliang@hit.edu.cn, TEL: +86-451 8640 2683, FAX: +86-451 8641 5244

Abstract

In the present work, the diamond wear mechanism during the scratching test is studied by Raman spectroscopy, backscattering electron scanning microscope (BSEM), energy dispersive X-ray spectroscopy (EDS) and X ray photoelectron spectroscopy (XPS). As the impact pressure reached the fracture strength of the diamond, surface chipping of the diamond grits occurred as the dominated diamond wear mechanism, which resulted in the formation of scattered micro diamond flakes on WC/Co surface. The transformation of diamond to graphite and oxidation of graphite are identified at the chip formation stage during the diamond scratching of WC/Co. In addition, the formation of tetrahedrally bonded amorphous carbon phase is proposed as new wear mechanisms under the dynamic loads.

Keywords: Diamond wear; Scratching; Phase transformation; WC/Co

1. Introduction

Diamond is now widely used in the manufacturing industry for its great hardness and good reliability. However, the wear of diamond tool in the machining process bears great impact on the form accuracy and surface integrity of the machined surface. A number of studies have been undertaken to study the phase transformation of diamond under the quasi-static loads (indentation test) and the mechanical failure during the machining process[1-4]. Actually, the wear mechanism was found to be dependent on both the material type and the loading conditions, such as the chemical reaction in machining Si and steel [5, 6], graphitization under high pressure [3, 7], as well as micro or macro fracture during the machining process [8]. However, few research was conducted on the combining effects of the friction induced temperature and high pressure during the dynamic loading condition [9, 10]. Under the high loading speed, micro-fracture and graphitization of the sharp tip can be induced, and the chemical wear under the dynamic loading condition become even more serious [11, 12]. Actually, the temperature of the cutting zone could reach even 1000 ℃, and more serious thermal damage of diamond can be induced at around 700-800 ℃ by the physical interaction [13, 14]. In addition, the oxygen environment aggravated the diamond wear, where oxygen-carbon-metal reaction was more energetically favorable [12, 15], but it has been rarely discussed to investigate the diamond tool wear in the precision machining field. Therefore, a further insight into the wear mechanism of diamond during the dynamic scratching is still of great necessity.

Raman spectroscopy has become a standard tool to characterize the carbon

materials, in which the appearance of the resonant peak is a good indication of different carbon material [16, 17]. The interpretation of the Raman shift peak, especially for the new emerged peaks, is of great significance [18, 19]. Specifically, diamond is characterized by a sharp Raman peak at around 1332 cm^{-1}, while graphite has two broad G, D band centered at 1575 and 1360 cm^{-1}, respectively. The specific position for D and G peak is dependent on not only the phase structure, but also the size of the diamond crystals, the stress state and the wavelength of the laser used [20-23].

In the present study, high speed diamond scratching of WC/Co is undertaken to get a systematic insight into the diamond wear mechanism under dynamic loading, considering both the physical and chemical aspects. Raman spectroscopy is applied to investigate the scratched WC/Co groove and the diamond grits after scratching, combining with the backscattering electron scanning microscopy (BSE), the energy dispersive X-ray spectroscopy (EDS) and the X ray photoelectron spectroscopy (XPS).

2. Materials and methods

2.1 Materials

Commercially available WC/Co carbide (Goodfellow Cambridge Ltd., UK) was chosen as the workpiece material. To manufacture WC/Co carbide, 6 wt.% cobalt is added into the WC powder green body, in which the diameter of WC grain is about 2 μm. Before the scratching test, the WC/Co material was firstly polished with the diamond paste of 1 μm diameter to remove the surface layer and reduce the impact of

the original surface defect. As shown in Fig. 1(a), the surface morphology of the WC/Co substrate after polishing indicates that the microstructure WC/Co has low porosity and fine grain. The roughness (R_a) of the polished surface is about 3 nm for WC/Co, as shown in Fig. 1(b). Table 1 lists the detail mechanical properties of the WC/Co composite provided by the manufacturer.

Table 1 Detailed mechanical properties for WC/Co

Elastic modulus E (GPa)	600
Vickers hardness H (GPa)	15.19
Fracture toughness K_{IC} (MPa $m^{1/2}$)	11.0
Compressive strength (MPa)	5500
Binder content (wt.%)	Co~6.0
Density ρ (g/cm^3)	14.95
Size of workpiece (mm)	12×12×5

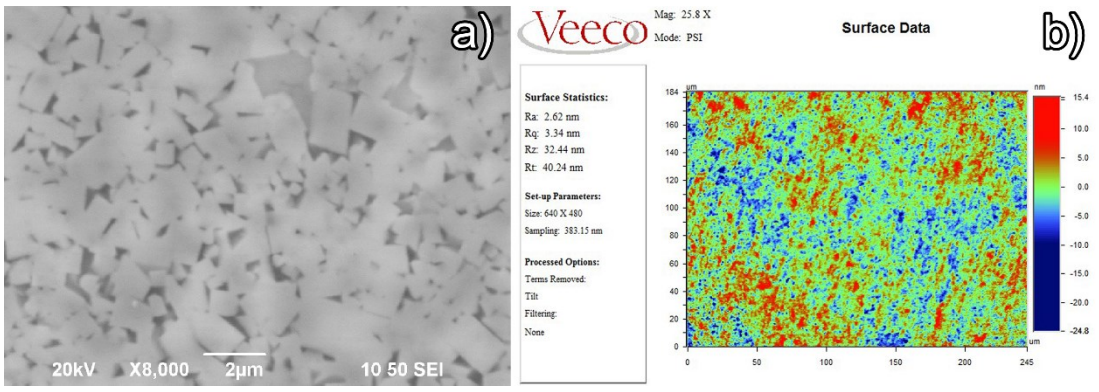

Fig. 1 Surface morphology and topography of the polished WC/Co material

2.2 Experimental methods

Dry scratching test was performed on a precision grinding machine (MUGK7120X5 Hangzhou Machine Tool Group Co., Ltd., China), equipped with three linear slides (X, Y and Z) and one main spindle (C). The maximum stroke of the horizontal X and Z slides is 500 and 200 mm, respectively. The minimum feed of vertical Y slide is 0.1 μm. The coolant was not provided to clearly observe the

morphology of the generated chips. The diamond grit was fixed to a steel disc and the rotational diameter of the sharp point was ~230 mm. A counter-part was also fixed on the steel disc to balance the system. The scratching test is illustrated in Fig. 2, and the detail scratching parameters is tabulated in Table 2. As shown in Fig. 2, the scratching speed (v_s) consisted of two parts, the feed of the workpiece (v_f) and the rotation of the diamond indenter (v_r), which can be calculated according to Eq. (1),

$$v_s = v_r + v_f = 2\pi \cdot n \cdot r + v_f \quad (1)$$

where v_s is the scratching speed, v_r is the rotation speed of the diamond indenter, v_f is the feed speed, n is the rotation speed of the indenter and r is the rotational radius of the indenter. The scratching speed is calculated to be 37.11 m/min according to the parameters in Table 2.

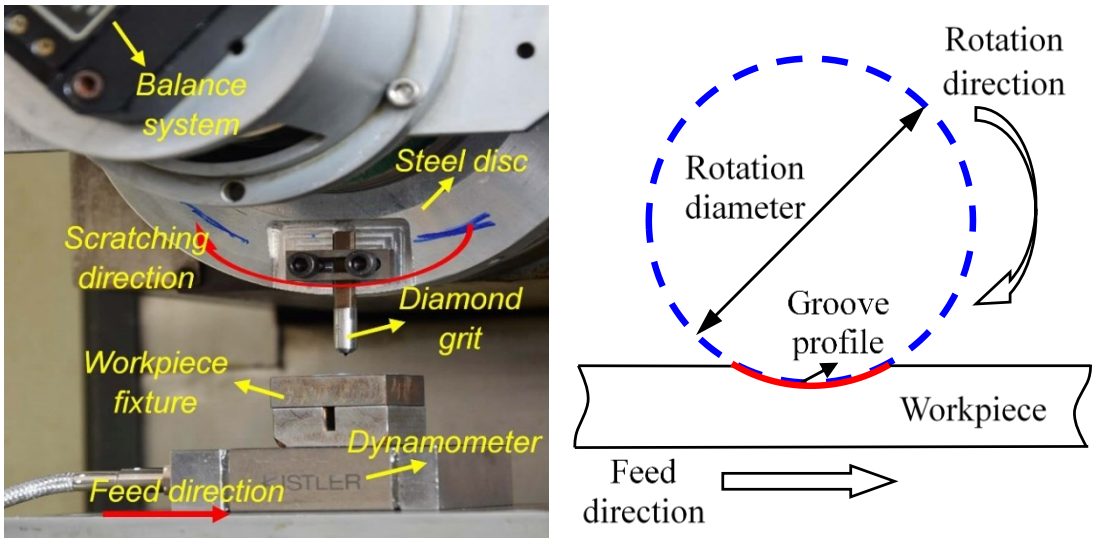

Fig. 2 Illustration of the scratching test

Table 2 Detailed scratching parameters

Machine	MUGK7120X5
Grit shape	Face to face apex angle 120°
Rotation diameter	230 mm
Rotation speed	50 RPM
Feed rate	1000 mm/min

The surface roughness of the polished WC/Co surface was measured by a white light interferometer (Wyko NT8000) with phase shifting interferometry in a range of 245×184 μm. The surface morphology of the indenter and the scratching groove was examined by a scanning electron microscope (SEM, JEOL Model JSM-6490) equipped with energy disperse spectroscopy (EDS), where the secondary electron imaging (SEI) was used to characterize the diamond grit surface and the backscattering electron imaging (BSE) was applied to examine the scratching groove. Raman spectroscopy was carried out on an Xplora system (Horiba) at room temperature. The confocal imaging resolution reaches submicron range, and the wavelength of the laser used was 532 nm, with the test time of 10 s for each under the SWIFT Co-Focus imaging mode. An average intensity of two times measurement was recorded with the 100× objective lens. Varied positions along the scratching groove were examined, as illustrated in Fig. 3. To compare with the points in the scratching grooves, point B on the polished WC/Co surface was also characterized, and the result is seen as the original material. In addition, X ray photoelectron spectrum (PHI 5400 ESCA System) of the diamond indenter after the scratching was collected to study the phase structure of the carbon materials.

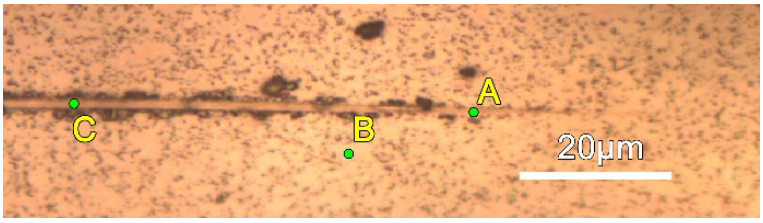

Fig. 3 Illustration of Raman spectra along the scratched groove

3. Results and discussion

From the surface morphology of the diamond grit after scratching shown in Fig. 4, it can be seen that the diamond indenter experienced obvious fracture which led to the generation of the random protruded sharp edges. The varied protrusion heights of these sharp tips resulted in the non-uniform cutting depth during scratching, as shown in Fig. 4(c) and (d) (Points A, B and D). The friction induced high temperature between the sharp tips with the workpiece material resulted in the oxidation, but it did not occur at the surface fracture point (C), as listed in Table 3.

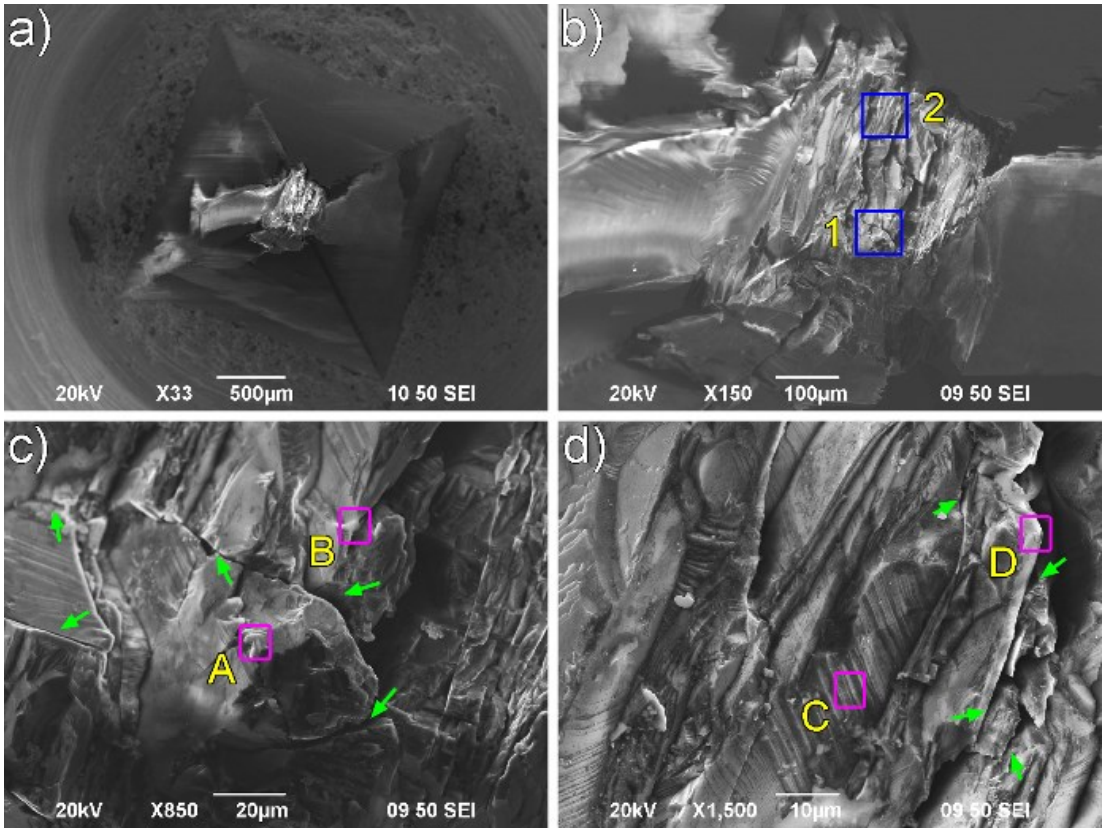

Fig. 4 SEM image of the diamond grits after scratching: (a) the overall appearance of the diamond grit; (b) the grit tip after scratching; (c) and (d) enlarged views of the diamond grits of area 1 and area 2

Table 3 Semi-quantitative EDS results for the points (A, B, C, D) in Fig. 4

Points	A	B	C	D
C	96.64	94.88	100	91.54

O	3.36	5.12	-	8.46

Fig. 5 shows the typical surface morphology of the scratching groove at three different cutting depths on WC/Co. From the surface morphology of the scratching groove shown in Fig. 5(a), it can be easily seen that only plastic scratching groove remained on the surface at the initial stage, without the formation of obvious chips and debris. With the increase of the cutting depth, discontinuous chips formed at the side of the grooves, as shown in the enlarged view from Fig. 5(a). The further increase of the cutting depth resulted in the formation of the continuous chips, and the side material along the groove is extruded to be uplifts, as shown in Fig. 5(b). The reciprocating wear test of WC/Co showed that the wear mechanisms are mainly plastic deformation, binder extrusion, WC grain fracture, grain dislodgement and surface crack [15, 24, 25]. The different mechanical properties between WC grains and Co binder resulted in the appearance of some pits due to the clearly deformed Co [15, 26]. The extrusion of WC grains and the formation of subsurface cracks can be induced during the multi-passes diamond scratching, and the fatigue of Co binder and its prior removal contributed to the WC dislodgement and the generation of cracks along the WC grain boundaries [15, 27, 28]. As far as the wear of the diamond indenter is concerned, the formed cutting edge due to the fracture of the diamond indenter participated in the material removal successively, even though the scratching test is undertaken in a single track in this study. As shown in Fig. 5, the bottom of the groove is covered by many finer ploughed grooves which is produced by the extrusion of the distributed sharp edges on the indenter after micro fracture. In addition, the transgranular fracture of WC grains resulted in many debris, some of

which embedded in the scratches caused by the rolling effects of the varied tips.

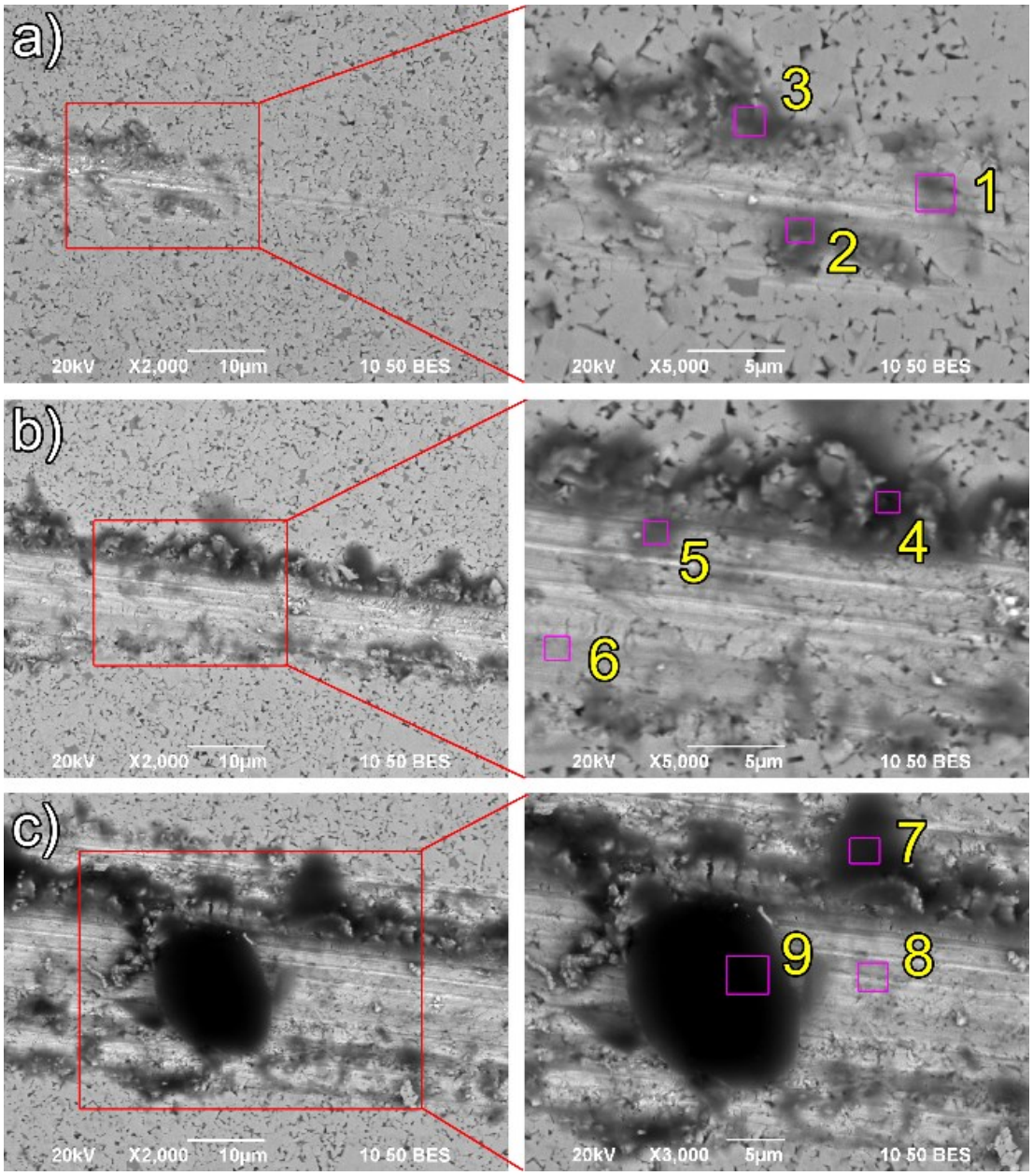

Fig. 5 BSEM image of the scratched grooves on WC/Co at different positions

It can also be found that the bottom of the scratches became densified under the compression of the indenter. The contrast between the WC grains and the Co binder becomes less clear due to the formation of a surface layer which was proposed to be composed of oxides and debris [15, 26, 29]. The adhesion of a layer of carbon materials should account for it to some degree in the present study, as some black

clusters were generated accompanied with the chips, as well as at the bottom of the scratching groove. The greater the cutting depth, the more black clusters generated. The EDS results for the thin black areas (1, 2, 3, 5, 6, 8), as listed in Table 4, indicates that the main component elements are C and O. Presumably, it should be attributed to the generation of graphite oxidation as the other possible oxidized products of carbon are gases [30]. The distribution of the C cluster attached to the chips further indicates the important role of the adhesion and friction between the diamond grit and chips. In addition, the black blocks of carbon material (4, 7, 9) also formed, as shown in Fig. 5(c). This is attributed to the serious abrasive effects of the WC chips and the accompanied high temperature. The flocculent shapes make us believe that they are different from the micro fracture induced chips of diamond.

Table 4 Semi-quantitative EDS results for the area 1-9 in Fig. 5

Element	C		O		W		Co		Others	
Position	wt.%	at.%	wt.%	at.%	wt.%	at.%	wt.%	at.%	wt.%	at.%
1	18.38	59.97	9.27	22.70	68.13	14.52	4.22	2.81	-	-
2	30.43	67.12	13.57	22.48	48.68	7.01	6.84	3.08	0.47	0.31
3	26.91	62.28	15.55	27.02	51.30	7.76	6.24	2.94	-	-
4	14.01	69.38	-	-	81.90	26.49	4.08	4.12	-	-
5	40.28	74.76	12.67	17.65	40.88	4.96	4.52	1.71	1.65	0.92
6	34.01	70.11	13.15	20.35	45.93	6.19	4.64	1.95	2.27	1.40
7	55.32	86.83	7.07	8.28	33.58	3.44	3.13	1.00	0.94	0.44
8	19.81	61.10	9.09	21.05	62.83	12.66	8.26	5.19	-	-
9	82.10	95.52	3.71	3.24	13.59	1.03	-	-	0.61	0.21

Obvious cracks also formed (indicated by green arrows in Fig. 4) on the diamond grit caused by the impact pressure, and the propagation trace remained on the surface, as shown in Fig. 4(c). The surface morphology of two typical scratching grooves at low magnification is shown in Fig. 6(a). For a fresh diamond indenter, the scratches

appear to be conformal with the indenter shape at the starting stage without considering the elastic deformation. With increasing depth of cut, surface fracture occurred, especially at the side of the grooves, which makes the groove profile irregular. After several times of scratching, the wear of the diamond indenter appeared, and the random fracture of the diamond tip resulted in the generation of the non-conformal grooves. It can be also found that some broken diamond chips distributed randomly near the scratched grooves. A typical diamond fragment is shown in Fig. 6(b), the thickness of which is estimated to be less than 1 μm, corresponding to the fracture layer thickness shown in Fig. 4(d). Due to the surface fracture of the diamond grits, more cutting edges formed, resulting in more finer grooves in the scratching grooves. The profile of the scratched grooves also changed with increasing cutting depth. Comparing with the attritious wear or large fracture, the micro fracture of the diamond grits contributes to the self-sharpness of the wheel during the grinding process, which promotes the cutting ability and contributes to the ductile material removal during the grinding of hard and brittle materials [31, 32].

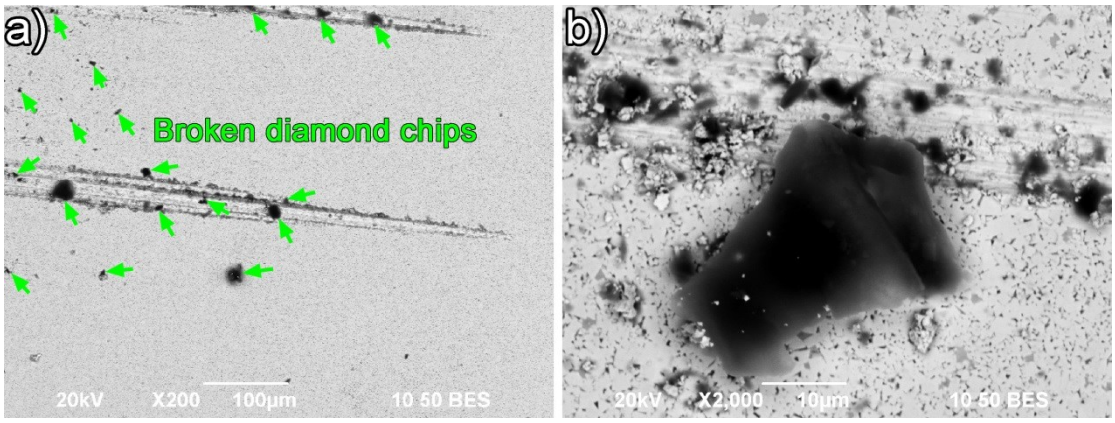

Fig. 6 Surface morphology of the scratches and the broken diamond chips scattered on WC/Co surface

To get further insight into the wear mechanism, the scratching grooves and the diamond grit after scratching test are characterized by Raman spectroscopy at varied points. The Raman spectra of the scratching groove, as shown in Fig. 7(a), indicates that the adhesion of the carbon materials appeared at some position of the scratched groove. In addition, three new Raman peaks also appeared for the worn diamond grit after the scratching. Specifically, the new peaks are centered at around 484.56 cm^{-1}, 1470.59 $cm^{-1}$and 1534.43 cm^{-1}, compared with the original diamond surface, as shown in Fig. 7(b). The diamond is characterized by a sharp Raman peak at around 1332 cm^{-1}, while graphite has two broad G, D band centered at 1575 and 1360 cm^{-1}, respectively. The surface of the diamond indenter and scratching groove should be composed of both diamond, graphite and other carbon materials under the high pressure and temperature condition. Therefore, the asymmetry shape of peak at around 1350.69 cm^{-1}, as shown in Fig. 7(c), is attributed to the D band of both the diamond and graphite, while 1534.43 cm^{-1} is the G band of the graphite and other carbon materials. More interestingly, the new peaks at around 484.56 cm^{-1} and 1470.59 cm^{-1} appeared, and the 1470.59 cm^{-1} peak is obviously separated rather than as the shoulder for the G-mode, which excluded the possibility of nanocrystalline diamond (NCD) [16]. In addition, the absence of 1140 cm^{-1} peak also ruled out the contribution from *trans*-$(CH)_x$ [33]. Referring to [22, 34], the appearance 484.56 cm^{-1} and 1470.59 cm^{-1} can be attributed to the formation of the tetrahedrally bonded amorphous carbon phase which corresponds to the simulated results based on Molecular dynamics [30].

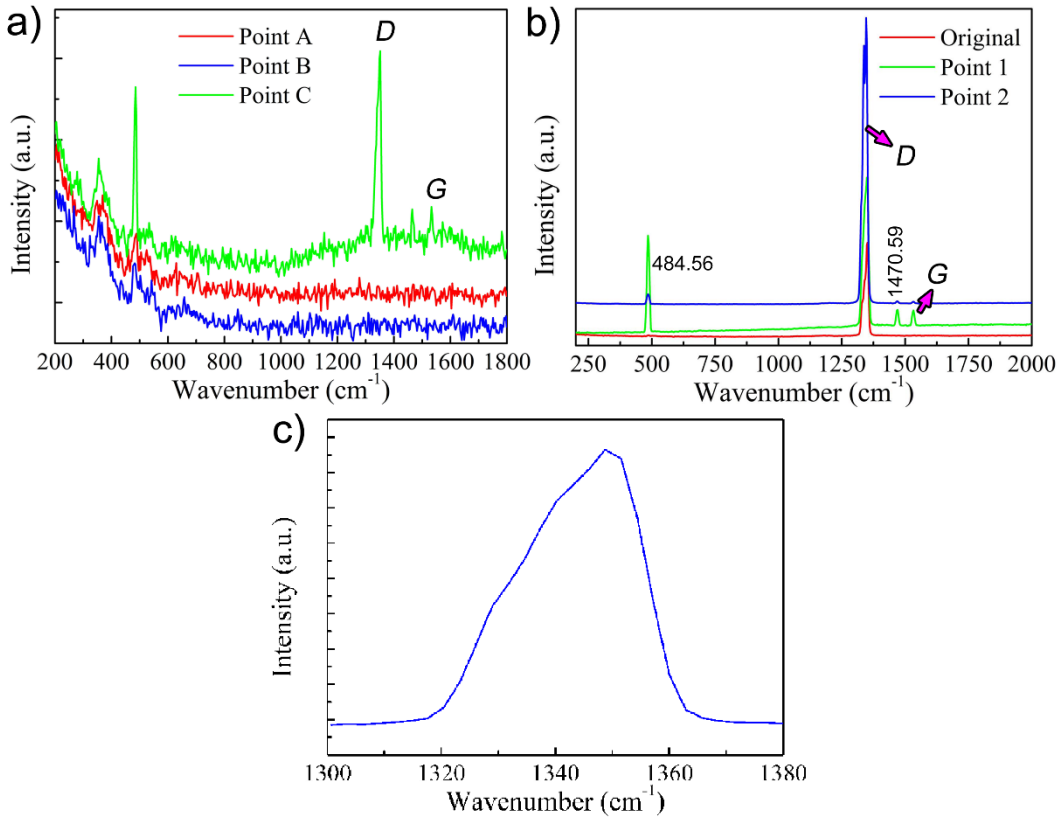

Fig. 7 (a) Raman spectra of the scratched WC/Co groove at three different points; (b) Raman spectra of the diamond grit after scratching test; (c) the D band peak of the indenter at point 1

The X ray photoelectron spectrum of the diamond indenter is shown in Fig. 8. It can be found from the full XPS spectra that C1s, N1s and O1s peaks were clearly detected. The formed C-N compounds was always found to be tetrahedrally bonded amorphous structure [35]. Presumably, it should be from the chemical reaction between the tetrahedrally bonded amorphous C or small graphite particle with the N_2 under the high pressure and high temperature during the scratching process [36, 37]. In addition, the two separated peaks around 284.5 eV and 286.5 eV is a good indication for the formation of graphite oxide [38, 39], as shown in Fig. 8(b).

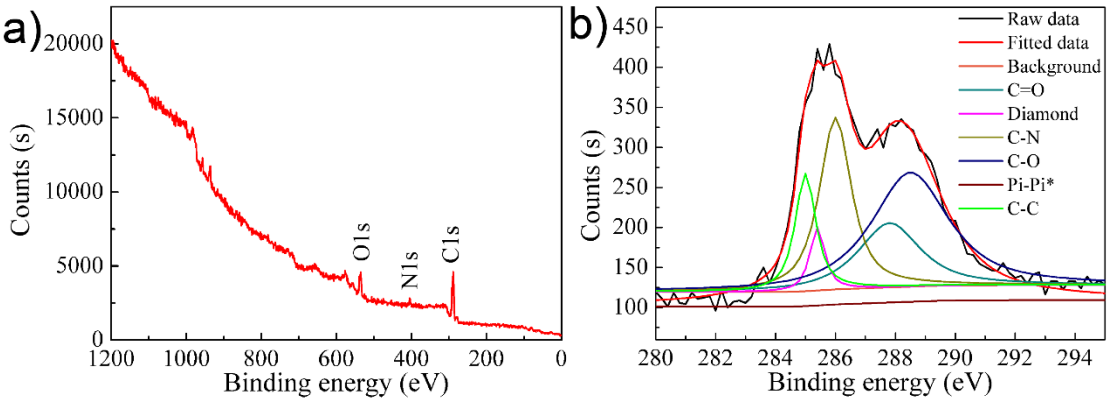

Fig. 8 (a) X ray photoelectron full spectrum of the diamond indenter after scratching test; (b) C1s spectrum

4. Conclusion

In summary, the diamond wear mechanism is investigated systematically in the present work. The micro fracture induced surface chipping is the main wear mode of the diamond grits under the dynamic scratching process, which occurred at a certain depth of scratching. The attritious wear also appeared obviously caused by the abrasive effects of WC chips. In addition, the transformation of diamond to graphitization and the formation of graphite oxide under dynamic pressure and high thermal loads were directly identified, and the transformation to tetrahedrally bonded amorphous carbon phase is experimentally verified as a new wear mechanism.

Acknowledgements

The work was supported by the Scientific Research Foundation of Nanjing University of Aeronautics and Astronautics and also the National Natural Science Foundation of China (NSFC) (Project No.:51475109 and 51275231).

References

[1] Z. Zhang, J. Yan, T. Kuriyagawa, Study on tool wear characteristics in diamond turning of reaction-bonded silicon carbide, Int. J. Adv. Manuf. Technol. 57 (2011)

117-125.

[2] L. Loisel, M. Châtelet, G. Giudicelli, M. Lebihain, Y. Yang, C. Cojocaru, A. Constantinescu, B.K. Tay, B. Lebental, Graphitization and amorphization of textured carbon using high-energy nanosecond laser pulses, Carbon 105 (2016) 227-232.

[3] Y.G. Gogotsi, A. Kailer, K.G. Nickel, Materials: transformation of diamond to graphite, Nature 401 (1999) 663-664.

[4] K. Aslantas, H.E. Hopa, M. Percin, İ. Ucun, A. Çicek, Cutting performance of nano-crystalline diamond (NCD) coating in micro-milling of Ti6Al4V alloy, Precis. Eng. 45 (2016) 55-66.

[5] S. Goel, X. Luo, R.L. Reuben, Wear mechanism of diamond tools against single crystal silicon in single point diamond turning process, Tribol. Int. 57 (2013) 272-281.

[6] Y. Wang, Q. Zhao, Y. Shang, P. Lv, B. Guo, L. Zhao, Ultra-precision machining of Fresnel microstructure on die steel using single crystal diamond tool, J. Mater. Process. Technol. 211 (2011) 2152-2159.

[7] R. Narulkar, S. Bukkapatnam, L.M. Raff, R. Komanduri, Graphitization as a precursor to wear of diamond in machining pure iron: a molecular dynamics investigation, Comp. Mater. Sci. 45 (2009) 358-366.

[8] G. Zhang, S. To, G. Xiao, Novel tool wear monitoring method in ultra-precision raster milling using cutting chips, Precis. Eng. 38 (2014) 555-560.

[9] V. Kanyanta, A. Dormer, N. Murphy, A. Invankovic, Impact fatigue fracture of

polycrystalline diamond compact (PDC) cutters and the effect of microstructure, Int. J. Refract. Met. H. 46 (2014) 145-151.

[10] D. McNamara, D. Carolan, P. Alveen, N. Murphy, A. Ivanković, Effect of loading rate on the fracture toughness and failure mechanisms of polycrystalline diamond (PCD), Int. J. Refract. Met. H. 60 (2016) 1-10.

[11] W.J. Zong, T. Sun, D. Li, K. Cheng, Y.C. Liang, XPS analysis of the groove wearing marks on flank face of diamond tool in nanometric cutting of silicon wafer, Int. J. Mach. Tool. Manuf. 48 (2008) 1678-1687.

[12] E. Paul, C.J. Evans, A. Mangamelli, M.L. McGlauflin, R.S. Polvani, Chemical aspects of tool wear in single point diamond turning, Precis. Eng. 18 (1996) 4-19.

[13] R.M. Hooper, J.L. Henshall, A. Klopfer, The wear of polycrystalline diamond tools used in the cutting of metal matrix composites, Int. J. Refract. Met. H. 17 (1999) 103-109.

[14] R.T. Coelho, S. Yamada, D.K. Aspinwall, M. Wise, The application of polycrystalline diamond (PCD) tool materials when drilling and reaming aluminium based alloys including MMC, Int. J. Mach. Tool. Manuf. 35 (1995) 761-774.

[15] A.J. Gant, J.W. Nunn, M.G. Gee, D. Gorman, D.D. Gohil, L.P. Orkney, New perspectives in hardmetal abrasion simulation, Wear 376 (2017) 2-14.

[16] H. Kuzmany, R. Pfeiffer, N. Salk, B. Günther, The mystery of the 1140 cm^{-1} Raman line in nanocrystalline diamond films, Carbon 42 (2004) 911-917.

[17] J. Kürti, A. Grüneis, H. Kuzmany, V. Zólyomi, Origin of the fine structure of the

Raman *D* band in single-wall carbon nanotubes, Phys. Rev. Lett. 90 (2003) 157401.

[18] A.C. Ferrari, J. Robertson, Raman spectroscopy of amorphous, nanostructured, diamond-like carbon, and nanodiamond, Phil. Trans. R. Soc. Lond. A 362 (2004) 2477.

[19] J. Robertson, A.C. Ferrari, Interpretation of Raman spectra of disordered and amorphous carbon, Phys. Rev. B 61 (2000) 14095-14107.

[20] J. Wagner, C. Wild, P. Koidl, Resonance effects in Raman scattering from polycrystalline diamond films, Appl. Phys. Lett. 59 (1991) 779-781.

[21] V.N. Mochalin, O. Shenderova, D. Ho, Y. Gogotsi, The properties and applications of nanodiamonds, Nature Nanotech. 7 (2012) 11-23.

[22] J. Schwan, S. Ulrich, V. Batori, H. Ehrhardt, S. Silva, Raman spectroscopy on amorphous carbon films, J. Appl. Phys. 80 (1996) 440-447.

[23] D.S. Knight, W.B. White, Characterization of diamond films by Raman spectroscopy, J. Mater. Res. 4 (1989) 385-393.

[24] J. Larsen-Basse, Binder extrusion in sliding wear of WC-Co alloys, Wear 105 (1985) 247-256.

[25] A.J. Gant, M.G. Gee, B. Roebuck, Rotating wheel abrasion of WC/Co hardmetals, Wear 258 (2005) 178-188.

[26] M. Gee, K. Mingard, J. Nunn, B. Roebuck, A. Gant, In situ scratch testing and abrasion simulation of WC/Co, Int. J. Refract. Met. H. 62 (2017) 192-201.

[27] C. Pignie, M.G. Gee, J.W. Nunn, H. Jones, A.J. Gant, Simulation of abrasion to

WC/Co hardmetals using a micro-tribology test system, Wear 302 (2013) 1050-1057.

[28] A.J. Gant, M.G. Gee, D.D. Gohil, H.G. Jones, L.P. Orkney, Use of FIB/SEM to assess the tribo-corrosion of WC/Co hardmetals in model single point abrasion experiments, Tribol. Int. 68 (2013) 56-66.

[29] M.G. Gee, L. Nimishakavi, Model single point abrasion experiments on WC/Co hardmetals, Int. J. Refract. Met. H. 29 (2011) 1-9.

[30] L. Pastewka, S. Moser, P. Gumbsch, M. Moseler, Anisotropic mechanical amorphization drives wear in diamond, Nature Mater.10 (2011) 34-38.

[31] M. Fujimoto, Y. Ichida, Micro fracture behavior of cutting edges in grinding using single crystal cBN grains, Diam. Relat. Mater. 17 (2008) 1759-1763.

[32] K. Wegener, H.W. Hoffmeister, B. Karpuschewski, F. Kuster, W.C. Hahmann, M. Rabiey, Conditioning and monitoring of grinding wheels, CIRP Ann. - Manuf. Technol. 60 (2011) 757-777.

[33] F.B. Schügerl, H. Kuzmany, Optical modes of trans-polyacetylene, J. Chem. Phys. 74 (1981) 953-958.

[34] B. Marcus, L. Fayette, M. Mermoux, L. Abello, G. Lucazeau, Analysis of the structure of multi‐component carbon films by resonant Raman scattering, J. Appl. Phys. 76 (1994) 3463-3470.

[35] S.E. Rodil, S. Muhl, Bonding in amorphous carbon nitride, Diam. Relat. Mater. 13 (2004) 1521-1531.

[36] L. Yin, M. Li, G. Luo, J. Sui, J. Wang, Nanosized beta carbon nitride crystal

through mechanochemical reaction, Chem. Phys. Lett. 369 (2003) 483-489.

[37] J. Robertson, C.A. Davis, Nitrogen doping of tetrahedral amorphous carbon, Diam. Relat. Mater. 4 (1995) 441-444.

[38] W. Gao, L.B. Alemany, L. Ci, P.M. Ajayan, New insights into the structure and reduction of graphite oxide, Nature Chem. 1 (2009) 403-408.

[39] S. Park, J. An, J.R. Potts, A. Velamakanni, S. Murali, R.S. Ruoff, Hydrazine-reduction of graphite- and graphene oxide, Carbon 49 (2011) 3019-3023.